20^{th} Annual Workshop on
Mathematical Problems in Industry
University of Delaware, June 21–25, 2004

Analysis of Pressurized Porous Air Bearings

Problem presented by
Drew Devitt, President
NewWay Precision Air Bearings Inc
Aston, PA 19014

	P. Evans	T. Fleetman	G. Goldsztein
	M. Froehlich	A. Jiang	C. McNally
Participants:	K. Orben	S. Rupani	G. Schleiniger
	D. Schwendeman	S. Swaninathan	A. Vasilic
	C. Williams	T. Witelski	

Summary Presentation given by D. Schwendeman (6/18/04)
Summary Report prepared by T. Witelski, D. Schwendeman, and P. Evans
(2/23/05 Final version)

1 Introduction

Mechanical systems requiring great precision in positioning of moving components can benefit from the use of externally pressurized air bearings. Pressurized bearings maintain finite separations between mechanical components by virtue of a lift force created by a pressurized flow of air through thin gaps between the components. A common everyday example is an air hockey table, where a puck is levitated above the table by an array of vertical jets of air. Using pressurized bearings there is no contact between moving parts and hence there is no direct solid-solid friction and theoretically no wear of sensitive components. This also suggests that pressurized bearings have very low effective drag and allow for designs that minimize the energy needed to move mechanical components.

This workshop project is focused on questions related to the design of porous air bearings produced by NewWay Precision Air Bearings Inc, see Figure 1. In these designs, one surface of the bearing is composed of a layer of porous material (a graphite foam). Pressurized air is pumped through this porous layer into the gap. Going through the porous layer causes the air flow to be more uniformly distributed than previous conventional designs, which supplied the air through a small number of orifices. This porous "diffuser" design is expected to yield bearings with better stability, lift, stiffness, and other characteristics, as described by [4, 7, 9]. Here we examine the mathematical equations for the lubrication theory models of these bearing designs. The simplified fluid dynamics given by these mathematical models can be used to predict the properties and design-parameter dependence for the bearings.

We consider two designs:

1. Pressurized porous slider bearings (the "puck" problem), see Figure 1(a,b).

2. Pressurized porous journal bearings (the bushing problem), see Figure 1(c).

For the puck problem we formulate a mathematical problem that describes the air flow through the porous layer and the air bearing gap. For the bushing problem we consider the heat flow in the

(a) (b) (c)

Figure 1: (a,b) Circular and slab geometry porous slider bearings, and (c) porous air bushings (Images from `www.newwayprecision.com`).

system and formulate a mathematical problem for the temperature in the porous journal bearing, the air gap and the metal shaft inside the bearing.

2 Derivation of the governing equations

The main properties that we will seek to predict for the slider bearings are their lift force and drag as functions of the input pressure and other slider parameters. The lift and drag will be determined from the coupled flow in the porous layer and the thin bearing gap.

2.1 Lubrication theory for the flow in the gap

For the relatively slow flow of air in the thin gap, the Reynolds number is small, and we may reduce the Navier-Stokes equations to a simplified lubrication flow [10]. As shown in Figure 2, we will idealize the bearing geometry. We will consider the porous slider to be a fixed horizontal surface parallel to the lower solid surface moving with speed U. The size of the slider is given by length scale L and the gap has constant height H.

The Navier-Stokes equations for the compressible air flow in the gap, $0 \le z \le H$, are

$$\rho \frac{D\vec{\mathbf{u}}}{Dt} = -\nabla p + \mu \nabla^2 \vec{\mathbf{u}}, \qquad \frac{\partial \rho}{\partial t} + \nabla \cdot (\rho \vec{\mathbf{u}}) = 0, \tag{1}$$

where ρ is the density, $\vec{\mathbf{u}}$ is the velocity field, and p is the pressure in excess of the standard atmospheric pressure (gauge pressure). For low Reynolds number flow, we can neglect the inertial terms, yielding the steady compressible Stokes equations

$$\vec{\mathbf{0}} = -\nabla p + \mu \nabla^2 \vec{\mathbf{u}}, \qquad \nabla \cdot (\rho \vec{\mathbf{u}}) = 0. \tag{2}$$

Then, for small aspect ratios, $H \ll L$, the lubrication limit reduces the Stokes equations to

$$0 = \frac{\partial p}{\partial z}, \qquad -\nabla_{\|} p + \mu \frac{\partial^2 \vec{\mathbf{u}}_{\|}}{\partial z^2} = 0, \qquad \nabla_{\|} \cdot (\rho \vec{\mathbf{u}}_{\|}) + \frac{\partial (\rho w)}{\partial z} = 0, \tag{3}$$

where we have separated the velocity into parts parallel to the solid surfaces and the perpendicular component, $\vec{\mathbf{u}} = \vec{\mathbf{u}}_{\|} + w\hat{\mathbf{k}}$, and $\nabla_{\|} \equiv (\partial_x, \partial_y)$. A consequence of the first equation in (3) is that the pressure is independent of the vertical direction, so that $p = p(x, y)$. Then the second equation in (3) can be integrated with respect to z subject to boundary conditions imposed on the velocity.

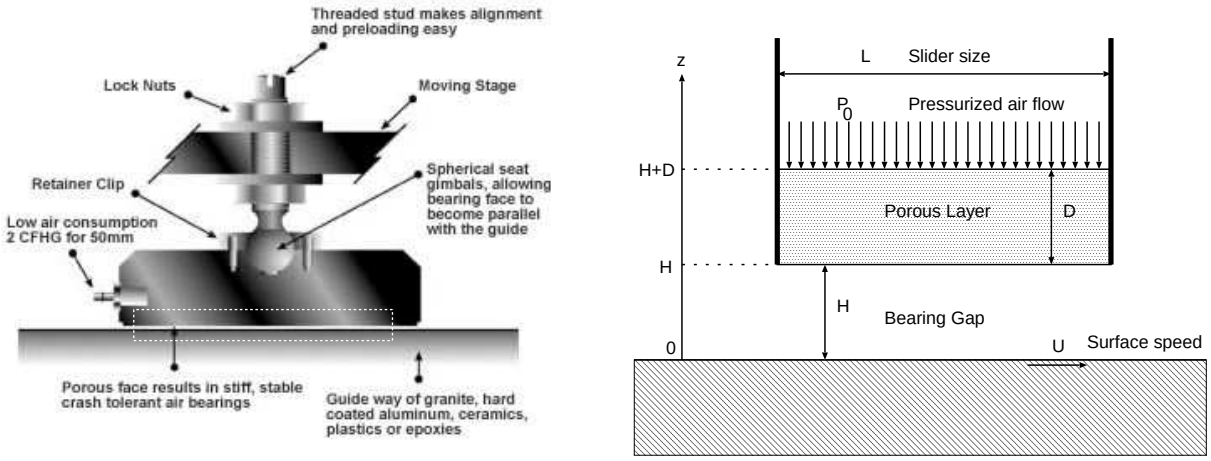

Figure 2: Schematic representations of the porous air bearing slider: (left) NewWay diagram of working configuration, (right) idealized representation of slider/air gap region (dashed-box in left figure).

These boundary conditions are taken to be: (i) no slip at the lower solid surface (moving with lateral velocity $\vec{\mathbf{U}}$),

$$\vec{\mathbf{u}}_{\parallel}(z=0) = \vec{\mathbf{U}}, \qquad w(z=0) = 0, \tag{4}$$

and at the porous slider surface: (ii) no lateral slip,

$$\vec{\mathbf{u}}_{\parallel}(z=H) = \vec{\mathbf{0}}, \tag{5}$$

with one remaining condition (on the normal component of velocity at the slider) that we will address shortly. We note that the influence of surface roughness (with amplitude much less than H) would introduce a negligible change to (4). Similarly, we neglect the influence of possible lateral slip at the porous surface; a model for slip boundary conditions at a porous surface was given by Beavers and Joseph [2], also described in [6, 8].

Consequently, the horizontal component of the gas velocity in the gap is given in terms of the pressure by

$$\vec{\mathbf{u}}_{\parallel}(x,y,z) = -\frac{\nabla_{\parallel} p}{2\mu} z(H-z) + \vec{\mathbf{U}}\left(1 - \frac{z}{H}\right), \qquad 0 \le z \le H. \tag{6}$$

While there is no direct contact and hence no solid-solid friction between the porous slider and the solid base surface, there is resistance to relative motion due to viscous drag on the gas in the gap between the surfaces. The drag on the moving surface due to the slider is given by the integral of the shear stress over the area of the slider,

$$\text{Drag} = \iint \hat{\mathbf{U}} \cdot \mu \frac{\partial \vec{\mathbf{u}}_{\parallel}}{\partial z}\bigg|_{z=0} dA \tag{7}$$

where $\hat{\mathbf{U}}$ is the unit direction vector for $\vec{\mathbf{U}}$, $\hat{\mathbf{U}} = \vec{\mathbf{U}}/|\vec{\mathbf{U}}|$, and the integral is evaluated over the base area of the slider. Using (6), together with the boundary condition that $p = 0$ at the edges of the slider, the drag reduces to the simple expression

$$\text{Drag} = \frac{\mu U}{H} \iint dA. \tag{8}$$

That is, for a fixed gap height H, the drag is proportional to the product of the sliding speed, $U = |\vec{\mathbf{U}}|$, and the slider area and inversely proportional to the gap height. This form of drag (the product of the viscosity, speed, and a geometric factor describing the problem) is expected from Stokes' law for drag in low Reynolds number flows.

The gap height itself is obtained from the equilibrium condition that the hydrodynamic lift balances the imposed load on the slider

$$\text{Load} = \iint p(x,y)\, dA. \tag{9}$$

As a result of this coupling of the load to the gap height, despite the fact that the Poiseuille term in (6) with explicit pressure-dependence, does not contribute to (8) the drag does implicitly depend on finding the pressure.

2.2 Air flow in the porous layer

We now turn to the problem of describing the air flow in the porous layer; this will be needed in order to obtain the pressure for (9). We consider the slider to be a layer of a homogeneous porous material with thickness D, on $H \le z \le H + D$. At $z = H + D$ we specify the imposed (gauge) pressure for the pressurized air flow, P_0. Within the layer, we model the flow as being governed by Darcy's law

$$\vec{\mathbf{u}}_{\text{porous}} = -\frac{k}{\mu}\nabla P \tag{10}$$

where $\vec{\mathbf{u}}_{\text{porous}}$ is the velocity field in the porous layer, $P(x,y,z)$ is the pressure in the porous layer and k is its permeability [1]. For a steady compressible flow the continuity equation is $\nabla\cdot(\rho\vec{\mathbf{u}}_{\text{porous}}) = 0$, and consequently the pressure satisfies an elliptic boundary value problem

$$\nabla\cdot(\rho\nabla P) = 0, \tag{11a}$$

$$P(z = H) = p(x,y), \qquad P(z = H + D) = P_0, \tag{11b}$$

and $\vec{\mathbf{n}}\cdot\nabla P = 0$ is imposed on the lateral surfaces of the porous layer, corresponding to no leakage of air out of the sides of the porous layer. The Dirichlet boundary condition on the upper surface of the porous layer represents the uniform pressure due to the imposed air flow. The boundary condition on the lower surface describes the continuity of the pressure at the interface between the porous layer and the lubrication gap.

2.3 Solving the coupled problem

Obtaining the drag, the equilibrium load and the gap height of the slider in terms of the imposed pressure P_0 involves solving the problems describes in Sections 2.1 and 2.2 as a coupled system. By the conservation of mass for the air flow, the vertical velocity into the gap at $z = H$ must match the velocity out of the porous layer. From (10) the local flux out of the porous layer gives

$$\rho w(z = H^-) = -\frac{\rho k}{\mu}\frac{\partial P}{\partial z}\bigg|_{z=H^+}. \tag{12}$$

This quantity must equal the flux into the gap, given by integrating the continuity equation $(3)_3$,

$$\rho w(z = H) = -\int_0^H \nabla_\parallel\cdot\left(\rho\vec{\mathbf{u}}_\parallel\right)\, dz = \frac{\nabla_\parallel\cdot(\rho\nabla_\parallel p)}{12\mu}H^3 + \frac{\nabla_\parallel\rho\cdot\vec{\mathbf{U}}}{2}H. \tag{13}$$

This yields the elliptic problem

$$\frac{\nabla_\parallel \cdot (\rho \nabla_\parallel p)}{12\mu} H^3 + \frac{\nabla_\parallel \rho \cdot \vec{\mathbf{U}}}{2} H = -\frac{\rho k}{\mu} \frac{\partial P}{\partial z}\bigg|_{z=H^+}, \tag{14}$$

with Dirichlet boundary conditions, $p = 0$, on the edges of the slider.

To summarize, for fixed $\vec{\mathbf{U}}$ and H, the problem reduces to solving (11) and (14) for $p(x, y)$ and $P(x, y, z)$, respectively. To completely specify the problem, a constitutive relation between the pressure and density must be supplied. Several possible cases may be considered, including, after appropriate non-dimensionalization:

- Incompressible flow

$$\rho = 1. \tag{15a}$$

- Compressible isothermal flow of an ideal gas

$$\rho = p. \tag{15b}$$

- Compressible adiabatic flow

$$p = \rho^\gamma, \quad \gamma > 1. \tag{15c}$$

The compressible cases yield challenging nonlinear problems. For simplicity, we consider only the linear problem resulting from the incompressible case; we show that despite neglecting compressibility of the air flow, this model yields results in good agreement with the experimental measurements.

3 Solutions of the slider problem

We now present solutions of the incompressible porous slider problem in two special cases: (1) the infinitely wide "slab" and (2) the axisymmetric "puck."

3.1 The one-dimensional slider problem

Consider rectangular sliders with $0 \le x \le L$ and $-W \le y \le W$. As described for (14), at the edges of the slider, the pressure vanishes. However, if we have a very wide slider, $W \gg L$, then we can hope to neglect the influence of the lateral boundary layers. That is, we can assume that for most of the area of the slider domain the solution is independent of y, i.e., $p = p(x)$ and $P = P(x, z)$. This assumption breaks down at $|y| = W$, but can be shown to lead to a small overestimate of the slider lift.

The reduced problem is

$$P_{xx} + P_{zz} = 0, \tag{16a}$$

on $0 \le x \le L$, $H \le z \le H + D$, where subscripts indicate partial differentiation. The boundary conditions are

$$P(x, H) = p(x), \qquad P(x, H + D) = P_0, \tag{16b}$$

$$P_x(0, z) = P_x(L, z) = 0, \tag{16c}$$

and on $0 \le x \le L$,

$$\frac{H^3}{12} \frac{d^2 p}{dx^2} = -k P_z(x, H) \tag{16d}$$

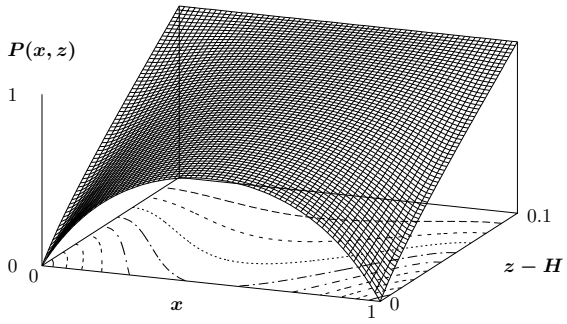

Figure 3: Numerical solution of problem (19) for $P(x, z)$ for a porous layer with thickness $D = 0.1$.

with boundary conditions

$$p(0) = p(L) = 0. \tag{16e}$$

If we regard $P(x, z)$ as known for the moment, then we may solve the sub-problem (16d, 16e) for $p(x)$ in terms of a convolution integral

$$p(x) = -\frac{12k}{H^3} \int_0^L G(x, s) P_z(s, H)\, ds, \tag{17}$$

where the Green's function for (16d) is

$$G(x, s) = -\frac{1}{L} \begin{cases} x(L - s) & 0 \le x \le s, \\ s(L - x) & s \le x \le L. \end{cases} \tag{18}$$

Since $p(x) = P(x, H)$, this can then be used to eliminate $p(x)$ from the coupled problem to yield an elliptic boundary value problem for $P(x, z)$ with an integral boundary condition on the lower edge:

$$P_{xx} + P_{zz} = 0, \tag{19a}$$

on $0 \le x \le L$, $H \le z \le H + D$, with boundary conditions

$$P(x, H) = -\frac{12k}{H^3} \int_0^L G(x, s) P_z(s, H)\, ds, \qquad P(x, H + D) = P_0 \tag{19b}$$

$$P_x(0, z) = P_x(L, z) = 0. \tag{19c}$$

A numerical code was written to solve this problem using a fast Poisson solver with a linear iterative method based on updating the form of the integral boundary condition, see Fig. 3.

If we make the assumption that the porous layer is very thin, $D \ll L$, so that there is a very small aspect ratio for the Darcy flow, then we can assume that to leading order P satisfies

$$\frac{d^2 P}{dz^2} = 0, \qquad H \le z \le H + D, \tag{20a}$$

$$P(x, H) = p(x), \qquad P(x, H + D) = P_0. \tag{20b}$$

The solution of this linear ODE is

$$P(x, z) = \frac{P_0}{D}(z - H) - \frac{p(x)}{D}(z - H - D). \tag{21}$$

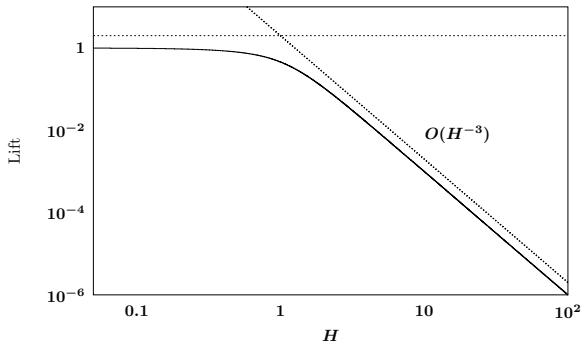

Figure 4: Lift vs. gap height for the one-dimensional porous slider shown on a log-log graph.

Consequently, we can eliminate P from (16d) to yield the boundary value problem for $p(x)$, namely

$$\frac{H^3}{12}\,p_{xx} - \frac{k}{D}p = -\frac{kP_0}{D}, \qquad p(0) = p(L) = 0. \tag{22}$$

The solution of this problem is

$$p(x) = P_0\left(1 - \frac{\cosh\big(\alpha(x - L/20)\big)}{\cosh(\alpha L/2)}\right), \qquad \alpha = \sqrt{\frac{12k}{H^3 D}}. \tag{23}$$

The lift force per unit width is then given by the explicit expression

$$F(H) = \int_0^L p(x)\,dx = P_0\left(L - \frac{2}{\alpha}\tanh(\alpha L/2)\right). \tag{24}$$

To understand the qualitative behavior of this result, we may consider the limiting behaviors for small and large gap heights

$$F(H) \sim \begin{cases} P_0 L & H \to 0, \\ P_0 L^3 D^{-1} H^{-3} & H \to \infty. \end{cases} \tag{25}$$

That is, for small gap heights, there is a maximum limiting load, $F_0 = P_0 L$, while for large gaps, the lift decreases like $1/H^3$, see Figure 4. Since the load is a monotone decreasing function of the gap height, this relation can be inverted to provide the relationship between the drag and the load for large H,

$$\text{Drag} \sim \mu U\left(\frac{FD}{P_0}\right)^{1/3}. \tag{26}$$

3.2 The circular slider problem

The analysis for an axisymmetric "puck" porous slider with radius R follows analogously. The argument leading to (21) for the pressure in the porous layer is unchanged. Writing (14) in cylindrical coordinates for $p = p(r)$ yields

$$\frac{H^3}{12}\,\frac{1}{r}\frac{d}{dr}\left(r\frac{dp}{dr}\right) - \frac{k}{D}p = -\frac{kP_0}{D}, \qquad p(0) \text{ bounded}, \qquad p(R) = 0. \tag{27}$$

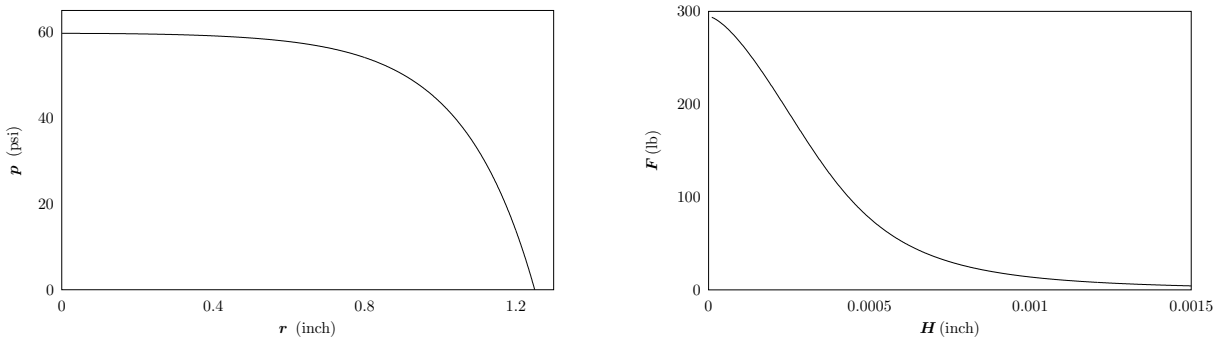

Figure 5: (Left) Pressure profile $p(r)$ and (right) lift as a function of gap height $F(H)$ for a typical porous puck with parameters $P_0 = 60$ psi, $R = 1.25$ in, $D = 0.187$ in, $H_0 = 0.0002$ in, $k = 4 \times 10^{-12}$ in^2.

The solution is

$$p(r) = P_0 \left(1 - \frac{\mathrm{I}_0(\alpha r)}{\mathrm{I}_0(\alpha R)}\right), \qquad \alpha = \sqrt{\frac{12k}{H^3 D}}, \tag{28}$$

where I_0 is the modified Bessel function of the first kind of order zero. The lift force is

$$F(H) = 2\pi \int_0^R p(r) r \, dr = P_0 \left(\pi R^2 - \frac{2\pi R \, \mathrm{I}_1(\alpha R)}{\alpha \, \mathrm{I}_0(\alpha R)}\right), \tag{29}$$

where I_1 is the modified Bessel function of the first kind of order one. Similar to (25), the limiting behaviors of the lift are

$$F(H) \sim \begin{cases} P_0 \pi R^2 & H \to 0, \\ P_0 \left(\frac{3\pi k R^4}{2D}\right) H^{-3} & H \to \infty. \end{cases} \tag{30}$$

The $H \to 0$ limit simply represents a direct balance between the pressure times the slider area and the load as to be expected. Let us define a friction or drag coefficient as the ratio

$$C_f = \frac{\text{Drag}}{\text{Load}}. \tag{31}$$

For the axisymmetric puck, this is given by

$$C_f = \frac{\mu U \pi R^2}{H F(H)} \sim \begin{cases} O(H^{-1}) & H \to 0, \\ O(H^2) & H \to \infty. \end{cases} \tag{32}$$

Note that C_f tends to infinity in both of these limits while it is finite for intermediate values of H. This implies the existence of a configuration with a local minimum for the drag coefficient. Figure 6 shows a log-linear plot of the drag coefficient for a slider with parameters given in Figure 5. The optimal load corresponding to a minimum drag coefficient, $F \approx 160$ lbs, is in good agreement with empirical results found at NewWay.

4 The porous bushing problem

The second problem considered in the MPI workshop concerned externally pressurized porous air bushings designed by NewWay. These are cylindrical shells of porous graphite that surround a

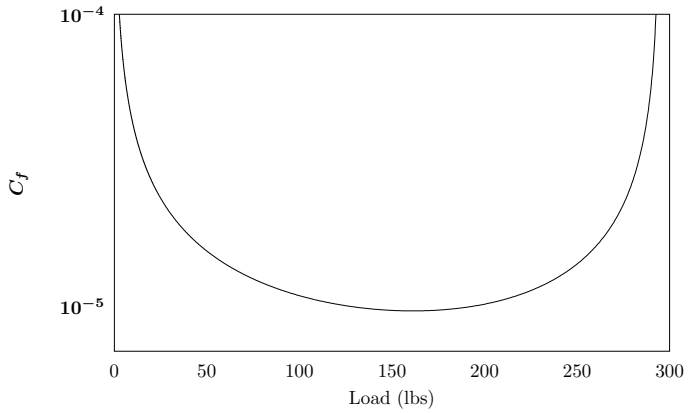

Figure 6: Drag coefficient for the circular slider described in Figure 5 subject to different loads. The minimum drag coefficient occurs at the optimal load of $F \approx 161\,\text{lbs}$.

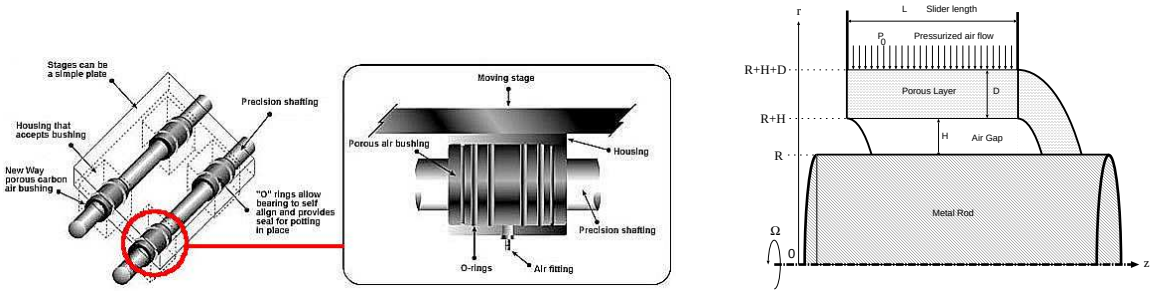

Figure 7: (Left) The porous bushing shown in operation as an element in a larger mechanical system [NewWay] and (right) a cross-sectional schematic of the bushing.

shaft rotating with angular velocity Ω, see Figure 7(left). Uniform axisymmetric air flow through the porous layer forces the shaft of radius R to remain centered in the bushing, separated by an annular gap of thickness H from the porous shell. The cross-sectional geometry of this problem is almost exactly the same as in the case of the one-dimensional slider, compare Figure 7(right) and Figure 2(right). In fact, when the radius of the cylinder is much larger than the thickness of the gap and the porous layer, so $R \gg H$ and $R \gg D$, then to leading order the effects of curvature are negligible and the results from Section 3 apply directly.

The questions of interest for the bushing problem relate to heat generation and heat transfer during operation. One significant difference from the puck problem is the nature of the relative motion between the porous and the the solid surfaces. In that problem the puck translates along a solid surface that can be assumed to be infinite in extent; it spends a very short time over any particular portion of the surface. In the bushing problem, the fixed porous shell surrounds a particular section of the rotating shaft; the same length of the shaft is covered by the bushing for the entire period of operation. Heat generated by the puck will be distributed over the whole solid surface and will readily dissipate. In contrast, heat generated by the bushing will accumulate locally in the enclosed section of the rotating shaft. If the shaft is made of a metal with a large thermal expansion coefficient, then the accompanying rise in temperature will cause the radius to expand, decreasing the air gap and possibly leading to catastrophic failure (seizure when the surfaces come into contact with $H \to 0$).

4.1 Steady state heat transfer

We analyze the steady state heat transfer [3, 5] through the porous bushing, the air gap and into the metal shaft. This involves a balance between dissipation of heat and production of heat. Heat is dissipated via conduction in the metal and porous graphite. Heat is produced by the viscous (i.e. frictional) flow of air: (1) through the porous medium and (2) in the Couette shear flow in the gap. For simplicity, we neglect heat loss due to convective heat transfer by the air flow. This is reasonable since with flow rate of air through the system is very small.

The leading order steady state solution is obtained by solving the coupled problems for the temperature in the central shaft, the air gap, and the porous shell:

1. In the shaft: In the shaft, the radial geometry is important, and the heat conduction problem for the temperature $T_s(r, z)$ must be solved in cylindrical coordinates

$$\frac{1}{r}\frac{\partial}{\partial r}\left(r\frac{\partial T_s}{\partial r}\right) + \frac{\partial^2 T_s}{\partial z^2} = 0 \tag{33}$$

on $0 \le r \le R$ and $0 \le z \le L$. The boundary conditions at the ends of the shaft will affect heat conduction out of the system. The proper choice of these conditions will depend on details of the geometry of the mechanical components exterior to the bushing. For convenience we consider the simple case of Dirichlet boundary conditions, describing the shaft being connected to perfect conductors (large heat sinks),

$$T_s(r, 0) = T_s(r, L) = 0, \qquad 0 \le r \le R. \tag{34}$$

Using separation of variables, the general solution of this problem can be written in the form

$$T_s(r, z) = \sum_{n=1}^{\infty} c_n \mathrm{I}_0(n\pi r/L)\sin(n\pi z/L), \qquad 0 \le r \le R, \tag{35}$$

where I_0 is the modified Bessel function of the first kind of order zero.

2. In the air gap: As described above, to simplify this problem, it is reasonable to assume that the air gap is very thin compared to the radius of the shaft, and also compared to the length of the shaft, i.e.

$$\frac{H}{L} \ll 1, \qquad \frac{H}{R} \ll 1. \tag{36}$$

The first assumption implies that the axial variation (z-dependence) can be neglected compared to the leading order r-dependence of the solution. The second assumption allows us to approximate the cylindrical form of the Laplacian operator with $\nabla^2 \sim \partial_{rr}$. Consequently the steady-state heat equation in the air gap is

$$K_a \frac{\partial^2 T_a}{\partial r^2} + \phi_a = 0, \qquad R \le r \le R + H, \tag{37}$$

where K_a is the thermal conductivity of the air and ϕ_a is the averaged volumetric heat production. This heat source term is given by the viscous dissipation due to the shear flow in the thin gap $H \ll 1$ at $r \sim R$

$$\phi_a \approx \frac{\mu}{2}\left(\frac{\Omega R}{H}\right)^2. \tag{38}$$

The general solution for the temperature $T_a(r,z)$ in the air gap is

$$T_a(r,z) = \frac{\phi_a}{2K_a}(r-R)(R+H-r) + \frac{T_0(z)}{H}(R+H-r) + \frac{T_1(z)}{H}(r-R), \tag{39}$$

where $T_0(z)$ is the temperature at the interface between the air and the shaft ($T_0(z) = T(R,z)$) and $T_1(z)$ is the temperature at the interface between the air and the porous layer ($T_1(z) = T(R+H,z)$), which are yet to be determined.

3. In the porous shell: We also assume that the porous layer is also thin relative to the dimensions of the shaft, so that the curvature of this layer may be neglected:

$$\frac{D}{L} \ll 1, \qquad \frac{D}{R} \ll 1. \tag{40}$$

Then, similarly, the steady-state heat equation in this layer is

$$K_p \frac{\partial^2 T_p}{\partial r^2} + \phi_p = 0, \qquad R+H \le r \le R+H+D, \tag{41}$$

where K_p is the thermal conductivity of the porous graphite and ϕ_p is the averaged volumetric rate of heat production. In porous materials, the rate of viscous dissipation of energy (equivalent to the loss of flow energy due to heat production) can be modeled by Poiseuille flow through pore channels

$$\phi_p = \frac{\beta \Delta p}{\text{Volume}} \approx \frac{\beta \Delta P}{2\pi RLD}, \tag{42}$$

where ΔP is a measure of the effective pressure drop across the porous layer and β is a constant related to the porosity. At the outer surface of the porous shell, we assume a convective cooling (Robin) boundary condition

$$\frac{\partial T_p}{\partial r} = -\alpha T_p, \qquad \text{for } r = R+H+D. \tag{43}$$

This condition includes the case of perfect insulation ($\alpha = 0$) as a special case. The solution of this problem for the temperature $T_p(r,z)$ in the porous layer is

$$T_p(r,z) = T_1(z) - \frac{\phi_p}{2K_p}(r-R-H)^2 + \left(\frac{D\phi_p}{K_p}\left[1 + \frac{\alpha D}{2}\right] - \alpha T_1(z) \right) \frac{r-R-H}{1+\alpha D} \tag{44}$$

where $T_p(R+H,z) = T_1(z)$.

Completing the solution of this system involves determining the interface temperature profiles, $T_0(z)$ and $T_1(z)$, by enforcing the continuity of the heat flux across $r = R$ and $r = R+H$. For example, at the interface between the porous layer and the air, we have

$$K_a \frac{\partial T_a}{\partial r}\bigg|_{r=(R+H)^-} = K_p \frac{\partial T_p}{\partial r}\bigg|_{r=(R+H)^+}. \tag{45}$$

Substituting (39) and (44) into this condition yields the following expression for $T_1(z)$ in terms of $T_0(z)$:

$$T_1(z) = \left(\frac{K_a}{H} + \frac{\alpha K_p}{1+\alpha D} \right)^{-1} \left(\frac{K_a}{H} T_0(z) + \frac{\phi_a H}{2} + \frac{\phi_p D}{1+\alpha D}\left[1 + \frac{\alpha D}{2}\right] \right) \tag{46}$$

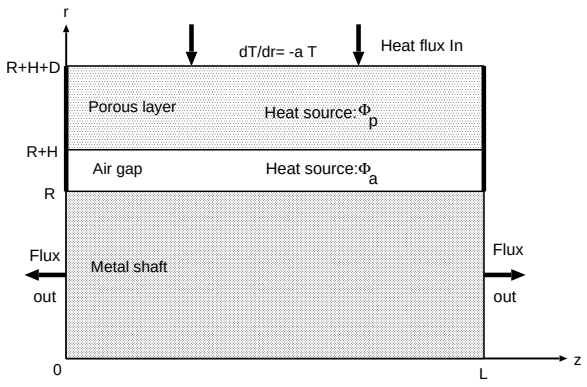

Figure 8: A schematic representation of the regions in the bushing heat transfer problem.

At the interface between the central shaft and the air, the continuity of the flux gives

$$K_s \frac{\partial T_s}{\partial r}\bigg|_{r=R^-} = K_a \frac{\partial T_a}{\partial r}\bigg|_{r=R^+}. \tag{47}$$

The flux out of the air gap is

$$K_a \frac{\partial T_a}{\partial r}\bigg|_{r=R^+} = K_a \left[\frac{\phi_a H}{2K_a} + \frac{T_1(z) - T_0(z)}{H}\right], \tag{48}$$

while the flux into the shaft is

$$K_s \frac{\partial T_s}{\partial r}\bigg|_{r=R^-} = K_s \sum_{n=1}^{\infty} \frac{n\pi}{L} c_n \mathrm{I}_1(n\pi R/L) \sin(n\pi z/L). \tag{49}$$

Also, the temperature at the surface of the shaft is

$$T_0(z) = \sum_{n=1}^{\infty} c_n \mathrm{I}_0(n\pi R/L) \sin(n\pi z/L). \tag{50}$$

Consequently, equating (48) and (49) and making use of (46) and (50) yields the expression

$$\sum_{n=1}^{\infty} b_n \sin(n\pi z/L) = \left(1 + \frac{\alpha H}{1+\alpha D}\frac{K_p}{K_a}\right)^{-1} \Big(\phi_a H \left[1 + \frac{\alpha K_p}{2K_a}\frac{H}{1+\alpha D}\right] + \frac{\phi_p D}{1+\alpha D}\left[1 + \frac{\alpha D}{2}\right]\Big), \tag{51}$$

where the coefficients b_n in the Fourier sine series are related to those in (50) by

$$b_n = \frac{K_s}{L} n\pi \mathrm{I}_1(n\pi R/L) c_n. \tag{52}$$

While (51) is long and cumbersome, it is essentially a Fourier sine series expansion of a constant (the right hand side is independent of z), and thus has the form

$$\sum_{n=1}^{\infty} b_n \sin(n\pi z/L) = \mathcal{F}, \tag{53}$$

where $\mathcal{F}$ is the constant on the right-hand-side of (51). Hence the series coefficients are given by

$$b_n = \frac{2}{L}\int_0^L \mathcal{F}\sin(n\pi z/L)\,dz = \frac{2\mathcal{F}}{n\pi}\left(1-\cos(n\pi)\right), \tag{54}$$

then the coefficients in (35) are

$$c_n = \frac{2L\mathcal{F}}{n^2\pi^2 K_s \mathrm{I}_1(n\pi R/L)}\left(1-\cos(n\pi)\right). \tag{55}$$

In the special case $\alpha = 0$, this formula simplifies to

$$c_n = \frac{2L(\phi_a H + \phi_p D)}{n^2\pi^2 K_s \mathrm{I}_1(n\pi R/L)}\left(1-\cos(n\pi)\right). \tag{56}$$

The contributions from heat generated in the porous layer $\phi_p D$ and the air gap ϕH are clear in this case.

Of particular interest is the rate of heat delivered at the ends of the shaft which must be dissipated in order to maintain a steady state. This power output is given by

$$\text{Power output} = 2\pi\int_0^R K_s\partial_z T_s(r,0) r\,dr = 2\pi R K_s\sum_{n=1}^{\infty} c_n \mathrm{I}_1(n\pi R/L), \tag{57}$$

where c_n is given by (55) in the case $\alpha > 0$ or (56) in the special case $\alpha = 0$. It is noted that for the special case of an otherwise thermally isolated system, $\alpha = 0$, the total power output is simply the total rate of heat generated in the system $4\pi RL(\phi_a H + \phi_p D)$, and for the case $\alpha > 0$ the power output given by (57) would be less due to some heat escaping through the outer boundary of the porous layer (at $r = R + H + D$).

4.2 Analysis of the critical time to failure

In the previous section, we determined a thermal balance in the system needed to maintain a steady heat flow. In that analysis, we assumed that heat was generated in the porous layer and in the air gap and that heat escaped at the ends of the metal shaft and at the outer boundary of the porous layer (if $\alpha > 0$). If, on the other hand, the heat generated does not escape fast enough, then the temperature of the system may become large and thermal expansion of the bushing parts may ultimately lead to failure as the air gap shrinks to zero. In order to analyze this behavior, we consider the radial expansion of the metal shaft due to thermal expansion and set

$$R = R_0 + \sigma T, \tag{58}$$

where R_0 is the radius of the shaft at a nominal temperature $T = 0$, say, and σ is the coefficient of thermal expansion for the metal. Let us assume for simplicity that the porous layer remains fixed so that as the metal shaft expands the air gap shrinks at the same rate. This assumption implies that

$$H = H_0 - \sigma T, \tag{59}$$

where H_0 is thickness of the air gap at the nominal temperature. Typically, there may be a small build-up of heat that ultimately leads to failure, but we consider the a worst case in which the system is fully insulated so that *all* of the heat generated raises the temperature and contributes to thermal expansion.

Assuming spatially uniform temperature in the metal shaft, we may write down a simple heat balance between the rate of change of heat energy within the shaft and the heat flux to the shaft at $r = R(t)$. This balance gives

$$\frac{d}{dt}\left[\rho_m c_m \pi L R^2(t) T(t)\right] = 2\pi R(t) L(\phi_a H + \phi_p D), \tag{60}$$

where ρ_m and c_m are the density and specific heat of the metal shaft, respectively, and with the initial conditions $T(0) = 0$. The derivative on the left hand side gives

$$\frac{d}{dt}R^2(t)T(t) = R^2\frac{dT}{dt} + 2RT\frac{dR}{dt} = \left(R^2 + 2R\sigma T\right)\frac{dT}{dt} \approx R_0^2\frac{dT}{dt}, \tag{61}$$

since $\sigma T \le H_0 \ll R_0$. Thus, (60) may be approximated by

$$\rho_m c_m \pi R_0^2 L\frac{dT}{dt} = 2\pi R_0 L(\phi_a H + \phi_p D), \tag{62}$$

or

$$\frac{dT}{dt} = k\left(1 + \frac{\phi_a H}{\phi_p D}\right), \qquad \text{where} \quad k = \frac{\phi_p D(2\pi R_0 L)}{\rho_m c_m(\pi R_0^2 L)}. \tag{63}$$

Formulas for ϕ_a and ϕ_p are given in (38) and (42), respectively, and these, using $R \approx R_0$, become

$$\phi_a = \frac{\mu}{2}\left(\frac{\Omega R_0}{H}\right)^2 \qquad \text{and} \qquad \phi_p = \frac{\beta\Delta P}{2\pi R_0 L D}. \tag{64}$$

Using (59) and (64), we may write (63) in the form

$$-\frac{1}{\sigma}\frac{dH}{dt} = k\left(1 + \frac{\eta}{H}\right), \qquad \eta = \left(\frac{\mu\Omega^2 R_0^2}{2}\right)\left(\frac{2\pi R_0 L}{\beta\Delta P}\right) \tag{65}$$

with $H(0) = H_0$.

We note in (65) that H decreases monotonically according to the sum of two terms. The first term is constant and is due to the heat generated in the porous layer, while the second term increases with decreasing H and is due to viscous heat generated in the air gap. An expression for the time to failure, t_c, may be found by regarding t as a function of H in (65) and then integrating from $H = H_0$ to $H = 0$. We find

$$t_c = \frac{1}{\sigma k}\left[H_0 - \eta\ln\left(1 + \frac{H_0}{\eta}\right)\right] \tag{66}$$

Figure 9 provides an interpretation of this result. Assuming that the heat generated in the porous layer is the dominant heat source, then (65) reduces to

$$-\frac{1}{\sigma}\frac{dH}{dt} \approx k \tag{67}$$

which implies a linear decrease in the thickness of the air gap given by

$$H \approx H_0 - \sigma k t \tag{68}$$

and an approximate time to failure $t_c \approx H_0/(\sigma k)$. This behavior is indicated by the dashed line in Figure 9. This approximation is valid provided $\eta/H \ll 1$ which ultimately breaks down when H approaches zero. As H approaches zero, the viscous heat generated in the air increases so that the approach to zero increases. The overall behavior of H versus time is indicated in the figure by the solid line, and the time to failure is marked.

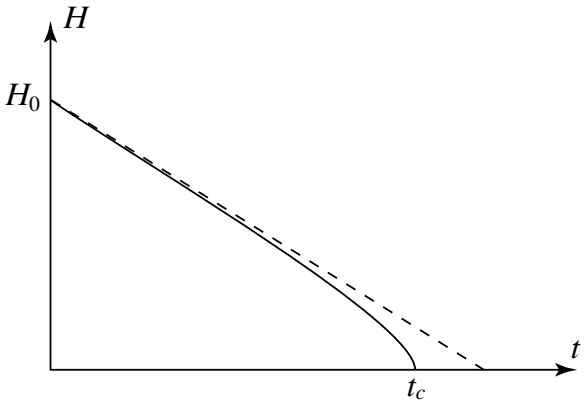

Figure 9: Behavior of the thickness of the air gap H versus time t, and the critical time to failure t_c.

5 Conclusions

Various mathematical models of the mechanical and thermal behavior of porous air bearing have been presented and analyzed in order to gain an improved understanding of porous air bearings. Lubrication theory allows the use of a relatively simple model for the flow of gas in the air gap, as the gap is extremely thin relative to the lateral size of a bearing. A model based on Darcy's law was used for flow through the porous layer. Our modeling of the air flow required a number of simplifications, such as assuming smooth parallel surfaces and an isotropic porous medium. These assumptions may be relaxed in order to produce more realistic results, but at the expense of a more complicated mathematical model. One assumption which may particularly limit our model is that of incompressible air flow through the porous layer; we did not assess what effect this would have on the bearing behavior. Combining our models for the air gap and porous layer, we were able to produce expressions for the load supported by the bearing, and the drag force. We found an expression for the drag coefficient involving slider speed, air viscosity, and the slider geometry. In particular, it appears there is an optimal gap width for which the drag coefficient is a minimum.

We modeled the heat generation in a porous bushing. Here, heat is generated by viscous dissipation and this heat must be removed to keep the parts of the bushing cool and avoid failure due to thermal expansion. We suggested that most of the cooling is provided by heat conduction into the bearing shaft. In particular we neglected the thermodynamics of the air flow; some small amount of heat is removed by convection of air out the air gap at the ends of the bushing. As a result of this analysis, we were able to estimate the time to failure when the bearing will seize.

Our modeling effort has produced good insight into the behavior of the porous bearings from very basic models. If the models can be validated against NewWay experimental results, and refined further if necessary, these could become useful tools for improved design and understanding of porous air bearings.

References

[1] J. Bear. *Dynamics of fluids in porous media.* American Elsevier, New York, 1972.

[2] G. S. Beavers and D. D. Joseph. Boundary condition at a natural permeable wall. *Journal of fluid mechanics*, 30:197–207, 1967.

[3] H. S. Carslaw and J. C. Jaeger. *Conduction of heat in solids*. The Clarendon Press Oxford University Press, New York, second edition, 1988.

[4] V. D. Djordjevic and C. Crnojevic. On the gas lubrication by injection through a permeable wall. *Facta Universitatis: Mechanics Automatic Control and Robotics*, 3(11):29–35, 2001.

[5] E. R. G. Eckert and R. M. Drake. *Analysis of heat and mass transfer*. McGraw-Hill, New York, 1972.

[6] A. A. Elsharkawy, S. Z. Kassab, and M. M. Nassar. Lubrication analysis of externally pressurized circular porous bearings. *Appl. Math. Modelling*, 20:870–876, 1996.

[7] M. Fourka and M. Bonis. Comparison between externally pressurized gas thrust bearings with different orifice and porous feeding systems. *Wear*, 210:311–317, 1997.

[8] J. K. Knudsen and K. E. Palmquist. The effect of porosity on the head-media interface. *Journal of Tribology*, 123:555–560, 2001.

[9] A. G. Montgomery and F. Sterry. A simple air bearing rotor for very high rotational speeds. In *UK atomic energy research establ. ED/R*, volume 1671. Harwell, Berkshire, England, 1955.

[10] J. R. Ockendon and H. Ockendon. *Viscous flow*. Cambridge University, Cambridge, 1995.